Neuroimaging with Functional Near Infrared Spectroscopy: from formation to interpretation

Javier Herrera-Vega[1,*], Carlos G. Treviño-Palacios[1], Felipe Orihuela-Espina[1]

[a]*Instituto Nacional de Astrofísica, Óptica y Electrónica,*
Luis Enrique Erro No.1 Sta. Maria Tonantzintla, Puebla, México

Abstract

Functional Near Infrared Spectroscopy (fNIRS) is gaining momentum as a functional neuroimaging modality to investigate the cerebral hemodynamics subsequent to neural metabolism. As other neuroimaging modalities, it is neuroscience's tool to understand brain systems functions at behaviour and cognitive levels. To extract useful knowledge from functional neuroimages it is critical to understand the series of transformations applied during the process of the information retrieval and how they bound the interpretation. This process starts with the irradiation of the head tissues with infrared light to obtain the raw neuroimage and proceeds with computational and statistical analysis revealing hidden associations between pixels intensities and neural activity encoded to end up with the explanation of some particular aspect regarding brain function.To comprehend the overall process involved in fNIRS there is extensive literature addressing each individual step separately. This paper overviews the complete transformation sequence through image formation, reconstruction and analysis to provide an insight of the final functional interpretation.

Keywords: fNIRS, image formation, reconstruction, image analysis.

1. Introduction

Neuroimages are either structural (anatomical) or functional (metabolic) images of the nervous system with special interest being those focusing on the brain. The term neuroimage encompasses different modalities of images formed from a range of physical processes whether electromagnetic e.g. [1] or mechanical e.g. [2]. Optical neuroimaging are the subset that exploits light for imaging the brain and its function, an endeavour that can be attempted in several fashions as exemplified *in-vivo* by optogenetics [3], or *ex-vivo* by see-through brain techniques such as CLARITY[1] [4] or Stimulated Emission Depletion (STED) nanoscopy in neuroscience [5]. Here we focus our description on the *in-vivo* brain images generated from diffuse optics.

Brain functional information can be observed through different constructs; metabolic (directly), electrophysiological and hemodynamic. Functional Near Infrared Spectroscopy (fNIRS) neuroimaging, indirectly senses the hemodynamic changes subsequent to neural activity. fNIRS for *in-vivo* brain function investigation [6, 7] is a versatile neuroimaging option that in general offers a good compromise between temporal and spatial resolution [8]. To elucidate brain function using fNIRS obtained from the processed data of a set of photodetectors it is of utmost importance to be acquaintance with how the diffuse optical neuroimage encodes the information related to the brain function. On this process each transformation on such data retrieves relevant information under particular assumptions which produces boundaries and limits the final interpretation.

On this paper an overview on how to obtain brain activity using diffuse optics. Specifically surveys the information path to decipher brain function from neuroimaging fNIRS recordings in order to make accurate interpretation. A quick overview on the fundamentals of fNIRS can be found in [9, 10, 11, 12, 13, 8, 14] further permitting a historical perspective. For an excellent compilation of the early stages of image formation and reconstruction in biomedical optics we suggest [15]. Excellent as they are, none of these however travel through the full lifecycle of information as this overview.

The information path can be mathematically ex-

*Corresponding author

[1]**C**lear **L**ipid-exchanged **A**crylamidehybridized **R**igid Imaging/immunostaining/in situ hybridization compatible **T**issue-h**Y**drogel

pressed as a succession of transformations across spaces re-expressing the information each time one step closer to expert knowledge. The transformations chain that neurological information undergoes from its metabolic origin until it is decoded by the neuroscientist is summarised in Figure 1. This path starts on a radiation source and ends up at the knowledge space, and can be expressed as a composition of functions. For simplicity, the roadmap of transformations is presented as a sequential process, but the actual journey may actually take some loops. The specific choice of transformations is somehow arbitrary admitting further detailing or coarser progression. Ideally, the transformations among the spaces will be mappings i.e. continuous and differentiable, guaranteeing that the algebraic structure is maintained and thus information topology is preserved, but this may not always be possible e.g. disambiguation of metamerism. Regardless, achieving appropriate interpretation requires careful consideration of all the transformations applied and new knowledge has to be bounded by the assumptions made in eachstep.

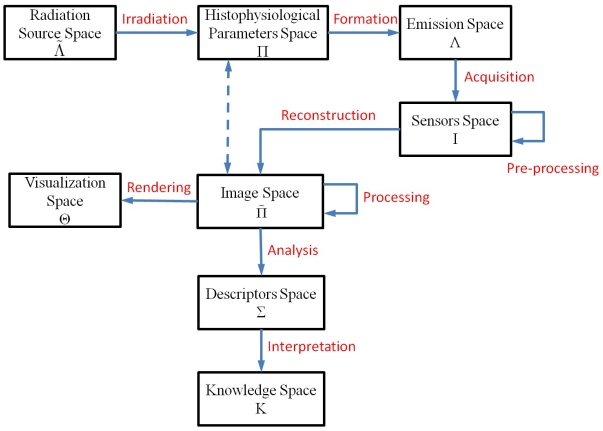

Figure 1: Schematic roadmap for fNIRS neuroimage interpretation. The greek letters identify the different informationspaces. A space is a set (collection of information) with an algebraic structure (set of operations or functions). Spaces contain information and transformation functions project information to the same (internal operation) or a different space (external operation). Different transformations relate one information space to another to complete the journey from the radiation source to the generation of knowledge. Each step can be mathematically formulated as a function between these spaces. The dashed line suggests that the image space is often a subspace of the histophysiological parameters space. The system dynamics varying with time T is "ghosted" for clarity.

2. Metabolic activity of the neuron, brain organizational principles and physico-chemical rules

Anatomically, the brain is one of the organs of the central nervous system (CNS) [16, 17] conformed by a complex network [18] of approximately 86 billion neurons and over 10^{14} connections among them [19]. Cytoarchitectonically many regions can be differentiated in the brain [20]. The histological differentiation of the cerebrum - part of the forebrain - into gray and white matter is of relevance for fNIRS. The gray matter contains the mayority of the neuron's somas and is where most information processing occurs, including cognitive processing. fNIRS neuroimage is confined to this cortical surface. In contrast, white matter is mainly composed of axons and its primary function is information transfer [21], encoded in an electrical signal.

The processing and transfer of information through neurons, i.e. brain function, is a metabolic process demanding energy that the neuron obtains from breaking glucose using oxygen [22]. Brain function is the reflection of the processes of gene expression and protein synthesis governing the neuron's life [23], the catabolic and anabolic paths for energy storing, transport and release [24], the chemiosmosis permitting neuron respiration [25] and ultimately the glucose consumption and oxidative metabolism [26, 27]. A neuron is active if it presents an electrical activity known as action potential [28, 29].

A complex vascular system irrigates the brain with blood, critically providing the oxygen and glucose needed for activity [30]. The *neurovascular coupling* phenomenon [31, 32, 33] explains the cerebral hemodynamics subsequent to local brain activity. Such hemodynamics is described in terms of the cerebral blood flow (CBF), cerebral blood volume (CBV), oxygen fraction extraction (OEF) and cerebral metabolic rate of oxygen ($CMRO_2$) [34] . Each one of these parameters have their regional or local and their global expression and describe the changes in the amount of oxygen in the blood irrigating the neurons and thus ruling the concentration of hemoglobin in its oxygenated (HbO_2) and reduced (HbR) species [35] observed by fNIRS. The information processing occurring at the gray matter level. The associated local hemodynamic changes ocurring in the vascular network are the sources of the fNIRS signal. The goal is to isolate and enhance this process during analysis. The neurovascular coupling is a non-linear process both temporally and spatially which further difficults the information pathway.

Brain function abides by the principles of segregation and integration [36]. Segregation refers to the fact that

each region of the brain is able to carry out one or a few independent specific tasks. Integration refers to the collaboration among the different brain regions to achieve more complex tasks through communication between them, known as brain connectivity [37]. Connectivity is commonly studied at three levels: structural, functional and effective. Structural or anatomical connectivity is mostly studied *in vivo* by means of diffusion weighted MRI [38]. Functional connectivity or non-causal coactivity, and effective connectivity or causal are studied by means of functional neuroimaging [39]. Associated to the conectivity is the brain plasticity. Brain plastic capabilities refers to the connectivity patterns at any level. Its dynamic [40] requiring longitudinal observations to determine whether Hebbian (activity dependent) or non-Hebbian (stabilization driven) synaptic changes ocurr [41]. In general neuroimages provide support for experiments addressing both types of neuroscientific questions: segregational or integrational.

Optical diffuse neuroimages can be obtain either directly through the so called fast optical signal [42, 43, 44, 45] or indirectly through the evoked hemodynamics [46, 47, 48, 49]. The observation of brain activity by optical diffuse methods means is further hidden by systemic components [47, 50, 51, 52] which is the baseline biological activity keeping the body alive. The systemic effect is an umbrella term including the cardiac rhythm [35], the circadian rhythm [53], or cerebral autoregulation among others [54].

3. Image formation and acquisition

Image formation in fNIRS is the physical process by which irradiated light interacts with tissue in turn encoding brain activity. This can be expressed mathematically as (Eq. 1):

$$f_{form,\mathbf{x}} : \tilde{\Lambda}, \Pi \rightarrow \Lambda \tag{1}$$

where the transformation $f_{form,\mathbf{x}}$ goes from the space of the light source ($\tilde{\Lambda}$) and the space of histophysiological compounds (Π) to the emission space (Λ), as depicted in figure 1,. The information encoding associated to brain activity can be sensed either directly or indirectly at a given detection locations $\mathbf{x}$ upon tissue illumination. We measure alterations of the optical properties induced by different physiological parameters [14]. Note that $\mathbf{x}$ represents the location of the channel instead of the photodetector location. In other word, $\mathbf{x}$ is associated to the nominal location of the tissue portion being sensed determined by the source-detector positions. The physical process involved is radiation transport [55, 56, 57, 58];radiation is transported through the tissue altering the spatial distribution of the scalar field.

The formation of an image $f_{form,\mathbf{x}}$ requires two basic elements [59]: (i) a radiation source radiation $I_{0,\hat{\mathbf{x}}}(t, \lambda)$, where $\hat{\mathbf{x}}$ is the position of the radiation source, t the time and λ the wavelength and (ii) a medium through which that radiation propagates exhibiting spectral remittance, $R_{\mathbf{x}}(\lambda) \in \Lambda$ as function of its composition $\pi \in \Pi$. In the case of fNIRS these composition refers to the biological tissue of the human head and its histo-physiology.

Image acquisition determines the encoding of a scene into an image. This is expressed as a transformation from the emission space (radiation leaving the tissue) Λ to the image space I defined by the sensors:

$$f_{acq,\mathbf{x},\theta_{k,\mathbf{x}}} : \Lambda \rightarrow I \tag{2}$$

During the image acquisition an arrange of wavelength dependent photodetectors $\Theta = \{\theta_{k,\mathbf{x}}\}$ capture the exiting radiation which is inverse proportional to the concentration of chromophores along the optical path associated to $\mathbf{x}$. Each of these sensors detects the light at a given wavelength with quantum efficiency $F_{\theta_{k,\mathbf{x}}}(\lambda)$.

After image acquisition and formation, the photodetector $\theta_{k,\mathbf{x}}(t)$ collects light at time t, according to Eq. 3:

$$\theta_{k,\mathbf{x}}(t) = \int I_{0,\hat{\mathbf{x}}}(t, \lambda) R_{\mathbf{x}}(\lambda) F_{\theta_{k,\mathbf{x}}}(\lambda) d\lambda \tag{3}$$

Raw optical images are hence three dimensional tensors $I(T, \mathbf{X}, \Theta)$ in time T, space $\mathbf{X}$ and optical responses $\Theta = \{\theta_{k,\mathbf{x}}\}$ in a given wavelength range $\lambda \in \Lambda$. Each element of the tensor is a function yielding the pixel value $\theta_{k,\mathbf{x}}(t)$. This tensor is represented in Figure 2.

In the digital era acquisition is followed by digitization. It involves the processes of sampling and quantization [61], that is mathematically expressed as a composition of two functions:

$$f_{digit} = f_{quant} \circ f_{samp,\theta_{k,\mathbf{x}}} \tag{4}$$

where $f_{samp,\theta_{k,\mathbf{x}}}$ is the sampling function for the given sensor and f_{quant} is the quantization function. Some common choices for these functions are illustrated in Figure 3.

Many factors diminish the quality of the image [62] and limit the different temporal, spatial, spectral and radiometric resolutions [63]. Some are physical such as Abbe's limit [64], that indicates the resolution limit impose by diffraction, and that governs the point spread function [65, 66]. However for fNIRS now days the sensing geometry is the most important limiting factor

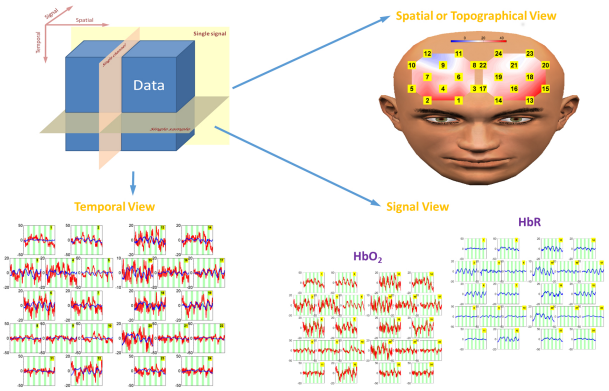

Figure 2: fNIRS neuroimage three dimensional tensor $I(T, \mathbf{X}, \Theta)$. T is the temporal component for either instantaneous events or dynamic processes. $\mathbf{X}$ is the spatial component collapsing all spatial dimensions of the Euclidean space of the scene. Θ describes the detector array response. $\mathbf{X}$ represents either topographical (2D) or tomographical (3D) images. Whenever the sensors are not arranged in a lattice they are referredas channels. Detector array positioning obey a particular imaging modality [60]: reflection or backscattering, transillumination or emission, or mixed as in coaxial or tomographic, both criteria perhaps imposed by the imaging modality. Cutting planes permits temporal, spatial and signal specific views and accordingly appropriate subsequent analysis.

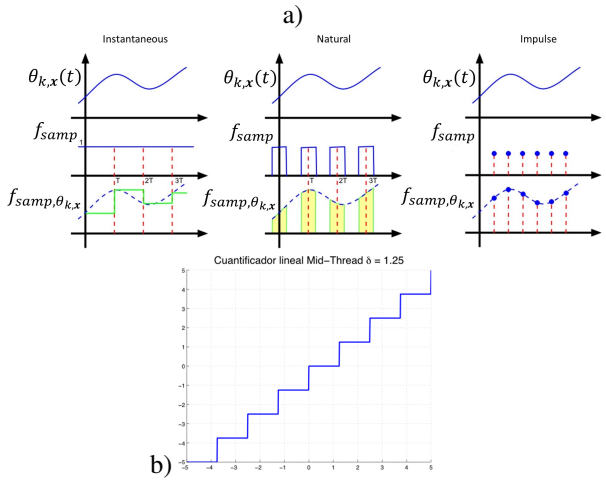

Figure 3: Image digitization $f_{digit} = f_{quant} \circ f_{samp,\theta_{k,\mathbf{X}}}$. Following sensing with the photodetector, the output electrical current is digitized, a process which involves sampling and quantization. a) Three common different sampling schemes $f_{samp,\theta_{k,\mathbf{X}}}$ b) A classical step function for quantization f_{quant} converting sampled sensor outputs to discrete digital values.

for spatial resolution images. Nevertheless high density diffuse optical tomography already offer at cortical depth exceptional resolution to the naked eye [67]. Other limiting factors are of biological origin such as the aformentioned systemic effect [51] or distortion provoked by heating [68]. Some are mechanical such as instrumental limits [69, 13] but these are continuously being pushed forward. In this regard, the latest wearable fNIRS devices incorporate features such as broadband illumination and sensing and the short-distance channel [70] to alleviate the extracerebral systemic influence using spectrally resolved spectroscopy [71] and becoming fibreless [72], or by obliquely reorienting fibers [73]. Some are environmental such as the movement of the tissue with respect to the sensors [74] or the reaching of ambient radiation to the sensor [62]. Some factors have numerical origin, such as the necessary discretization during sampling and digitization [61]. Finally, some may be demographic, such as the different concentration of chromophores and pigments in different races affecting the optical signal [75].

Diferent solutions improve image sensitity and resolution. Boas et al [6] summarise some of these: optimal selection of wavelengths [76, 77, 78, 79] to minimize random and systematic error propagation in the calculation of the hemoglobin concentrations, filtering of systemic physiological signal clutter to improve sensitivity to the hemodynamic response to brain activation [51, 80, 81, 82, 83], implementation of overlapping measurements during acquisition to improve image spatial resolution and uniformity [84, 85, 86, 87, 88], and the use of a priori spatial information from structural and functional magnetic resonance to reduce partial volume error [89, 90].

3.1. fNIRS forward modelling

fNIRS in either topographical [91] (2D) or tomographical [92] (3D) images of the tissue being imaged irradiates infrared light into the tissue and senses the exiting radiation after it has interacted with the tissues. The emissors and detectors are placed directly over the head and paired in channels. Detection is often performed using multiplexation a lock-in techniques. In the temporal doamin we can obtain static or dynamic images. Static refers to measuring the amount of scatterers through light extinction. Temporal dynamic measurements measures the motion of scatterers by electric field temporal autocorrelation function. The former exploits diffusion absorption spectroscopy and may be realized by irradiating tissue with three major spectroscopic schemes [93]. Static measurements are divided in continuous wave (CW) [31, 13], frequency domain [45] and time resolved [94]. Dynamic techniques are known also as diffuse wave spectroscopy techniques and may be realized by diffuse correlation spectroscopy [95].

In absorption spectroscopy, elaborated forward models solve different approximations of the radiation transport equation (RTE). These may be deterministic such as diffusion theory [55] or stochastic such as Monte Carlo based [96, 97, 98]. The computational implementation of the forward modelling with these methods involves the definition of a structural model of the tissues and the specification of optical properties for each tissue type for a set of wavelengths of interest. An example of forward modelling with Monte Carlo simulation of light propagation is shown in figure 4 in a mesh model of the human head.

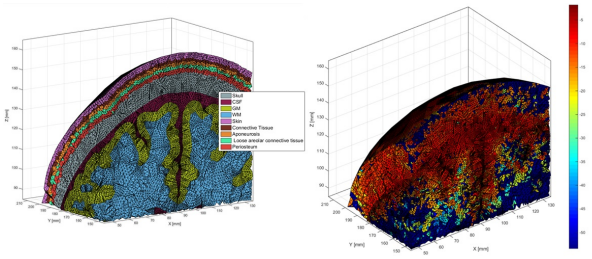

Figure 4: Left: An anatomical model of the adult human head based on a mesh showing its different tissues. Right: example of radiation propagation through the tissues of the head. A set of optical properties are assigned to every tissue which dictates the light propagation in the image formation process.

In the most basic scenario using CW modality and assuming perfect quantum efficiency$F_{\theta_{k,\mathbf{x}}}(\lambda) = 1$, attenuation is assumed to be the consequence of the alteration on the concentration of HbO_2 and HbR [8, 14] and expressed using the ubiquitous modified Beer-Lambert law [99, 100, 101] (Eq. 5).

$$\begin{aligned} \theta_{k,\mathbf{x}}: \quad & I(\lambda,t) = I_0(\lambda,t)e^{\mu_a(\lambda)\cdot d\cdot DPF(\lambda)+G} \\ \Rightarrow OD &= \ln\left(\frac{I(\lambda,t)}{I_0(\lambda,t)}\right) = \mu_a(\lambda)\cdot d\cdot DPF(\lambda)+G \end{aligned} \quad (5)$$

where $I_0(\lambda,t)$ is the light irradiated to the tissue characterizing the Irradiation Space $\tilde{\Lambda}$, $I(\lambda,t)$ is the intensity leaving the tissue (i.e. encoded in the Emission Space Λ), d is the interoptode distance, $DPF(\lambda)$ is the differential pathlength factor, G accounts for the (constant) complex geometry, $\mu_a(\lambda)$ is the macroscopic absorption coefficient, and OD stands for optical density and it is the ratio of exiting radiation with regards to input radiation. The unknown variable is $\mu_a(\lambda)$ as the tissue composition is ignored (which is precisely the task of reconstruction!). The $\mu_a(\lambda)$ is linearly approximated from the histophysiological parameters specific extinction coefficients $\varepsilon_p(\lambda)$ and their corresponding concentrations c_p plus some additional background macroscopic absorption $\mu_{a,bkg}(\lambda)$. When probing the cortex, d corresponds to an interoptode distance of approximately 3cm for adults [62] and 2cm for babies [102]. The $DPF(\lambda)$ [103, 77] accounts for the average extra length covered by the photons while travelling through the tissue due to scattering. Under the assumption of scattering being constant between two samples, it permits decoupling the scattering effects. Other than $\mu_a(\lambda)$, G is the only other term which is not known in the above equation.

4. Image reconstruction

Image reconstruction is the inverse process with respect to image formation [104, 105]. Image formation is dictated by physics; radiation is transported from the tissue to the sensors and in its trip encodes the physiological information of interest. Reconstruction is a mathematical process. It is represented as by (Eq. 6):

$$\tilde{f}^{-1}: I \rightarrow \tilde{\Pi} \quad (6)$$

It takes the information from the (digitized) sensors output $I(T,\mathbf{X},\Theta) = \tilde{f}(T,\mathbf{X},\Theta)$ and estimates a set of physiological parameters $P \in \tilde{\Pi}$, where $\tilde{f} \sim f_{digit} \circ f_{acq,\mathbf{x},\theta_{k,\mathbf{x}}} \circ f_{form,\mathbf{x}}$. The reconstruction process yields the familiar neuroimage that is function of physiological information $Y(T,\mathbf{X},P)$ by means of solving an ill-posed inverse problem as schematically depicted in Figure 5. Well posed problems in the Hadamard sense have an unique solution and this solution varies smoothly with the changes in the input. Ill-posed problems are those which may not have a unique solution because they violate the Hadamard assumptions. In fNIRS, the solution certainly exists since the tissue certainly has some specific optical, mechanical, and geometrical properties responsible for the observations. However, the solution to the inverse problem is not necessarily unique. This ambiguity solution is present in other cases, for example in metamerism [106, 107] illustrated in Figure 6. This ambiguity decreases the conditioning number of the Jacobian or sensitivity matrix that captures the (marginal) relations between the sensed data with respect to the variations of the parameters of interest bringing it closer to a zone of singularity.

Computationally, the solution of the image reconstruction problem is centered in alleviating these numerical instabilities. In one simple approach, the perturbation method [104], the solution vector with the parameters of interest is expressed from a nearby point and using Taylor series. Discarding the terms beyond the first

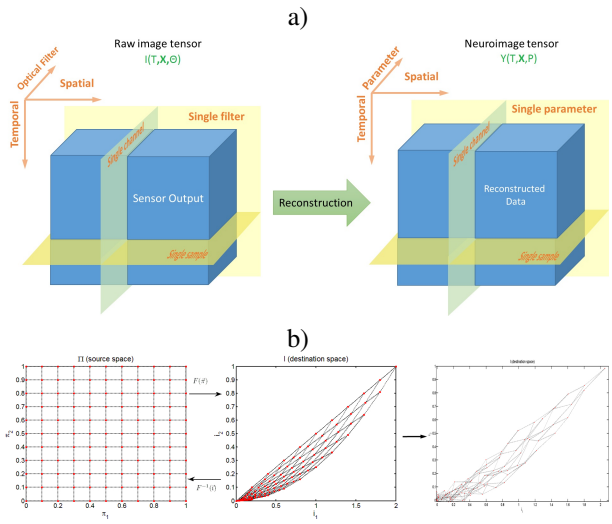

Figure 5: The image reconstruction process. a) The physiological information of interest is retrieved from the raw measurements through reconstruction, b) but the non-linear and noisy nature of the image formation render an ill-posed problem demanding regularization.

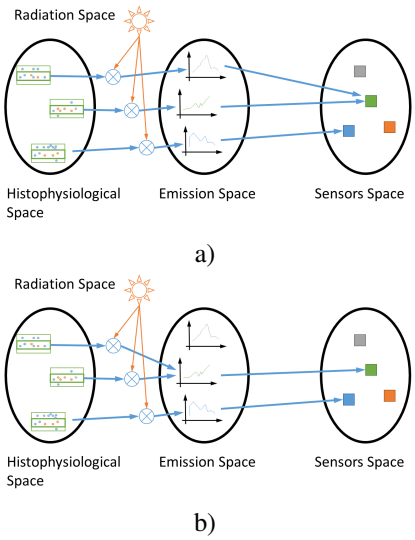

Figure 6: Metamerism, originally defined as the appreciation of the same color, was later generalized to the inability of a system to distinguish two different inputs [107]. It is the consequence of the inherent reduction in the dimensionality of the observed space imposed by the image acquisition process. a) Case I: The most common whereby two different spectral intensity distributions cannot be distinguished at sensor space, b) Case II: A less likely occurrence of the same output spectral intensity distribution from two different hystophysiological distributions.

derivative (that's the Jacobian), the reconstruction problems reduces to the calculation of the Jacobian. Since this is unstable for the reasons mentioned, regularization approaches are necessary [108, 109]. Perhaps the most common regularization approach in image reconstruction is Tikhonov [110] that in its most used form upsets the main diagonal of the matrix (like in the Levenberg-Marquardt method [108]). However, in the general case Tikhonov regularization upsets other elements of the matrix. A particularly useful approach to regularize the hypersensitivities often observed in regions near the optodes is to consider a spatial regularization factor [111]. The computational efficiency of the regularized reconstruction is also critical for real-time imaging [112]. To account for source and detector optode losses, calibration strategies can also be used [113, 114, 115].

Many fNIRS studies obviate these hinders posing relatively naive reconstruction solutions. In continuous wave fNIRS, reconstruction often involves simply solving a very simple system of equations generated differentially by forward modelling in terms of the modified Beer-Lambert law [99, 116, 101]. In the simplest case, n differential equations (for removal of the geometry term G) are formed at n acquisition nominal wavelengths $\lambda_1, \ldots, \lambda_n$. The changes in the unknown values Δy_n correspond to the changes in parameter p_n, and can be recovered according to Eq. 7:

$$\begin{bmatrix} \Delta i(\lambda_1) \\ \Delta i(\lambda_2) \\ \vdots \\ \Delta i(\lambda_n) \end{bmatrix} = \begin{bmatrix} \varepsilon_{p_1}(\lambda_1) & \varepsilon_{p_2}(\lambda_1) & \ldots & \varepsilon_{p_n}(\lambda_1) \\ \varepsilon_{p_1}(\lambda_2) & \varepsilon_{p_2}(\lambda_2) & \ldots & \varepsilon_{p_n}(\lambda_2) \\ \vdots & \vdots & \ddots & \vdots \\ \varepsilon_{p_1}(\lambda_n) & \varepsilon_{p_2}(\lambda_n) & \ldots & \varepsilon_{p_n}(\lambda_n) \end{bmatrix} \begin{bmatrix} \Delta y_1 \\ \Delta y_2 \\ \vdots \\ \Delta y_n \end{bmatrix} \tag{7}$$

Eq. 7 relates the raw image in the sensor output space I with the functional neuroimage in (neuro-)image space $\tilde{\Pi}$, $Y = \tilde{f}^{-1}(I)$. These approximations are not exact solutions to the radiation transport problem in biological tissue. This naive reconstruction ignores aspects such as inelastic multiple scattering or polarization, and further introduces new sources of errors e.g. cross talk [117, 118]. It is thus necessary to optimally select the irradiation and sensing wavelengths [76, 77, 78, 79, 119] as aforementioned. It corresponds to the researcher to decide whether the error of a certain reconstruction strategy is acceptable or he needs more aggressive solutions. A wide range of other techniques are available to address the image reconstruction process, for example, gradient-based or Newton-like methods [104, 120].

5. Image processing, analysis and interpretation

The analysis process $g : \tilde{\Pi} \rightarrow K, g = g_u \circ g_a \circ g_p(\tilde{f}^{-1})$ can be though in three levels; processing $g_p : \tilde{\Pi} \rightarrow \tilde{\Pi}$,

analysis $g_a : \tilde{\Pi} \rightarrow \Sigma$ and understanding or interpretation $g_u : \Sigma \rightarrow K$, with the limits between levels being fuzzy.

Processing, refers to those image transformations that result in another image with information of the same nature -the transformation codomain is the same as the domain-. The goal is often the separation of the neurosignal of interest from background noise [121, 52, 122]. In fNIRS, a typical processing flow as the one illustrated in Figure 7 may aim at correction of system drift through detrending, attenuation of systemic influence by means of decimation and boosting signal-to-noise ratio via averaging. Other traditionally relevant processing for fNIRS is the alleviation of optode (or body) movement artefact which has been attempted by different means [123, 74, 124, 62]. For example, the work of Scholkmann et al [125] presents a method to reduce movements artefacts by spline interpolation. Spatial and temporal processing often complement each other [126, 127, 128]. The term pre-processing is sometimes used interchangeably but most times is confined to refer to processing occurring before reconstruction.

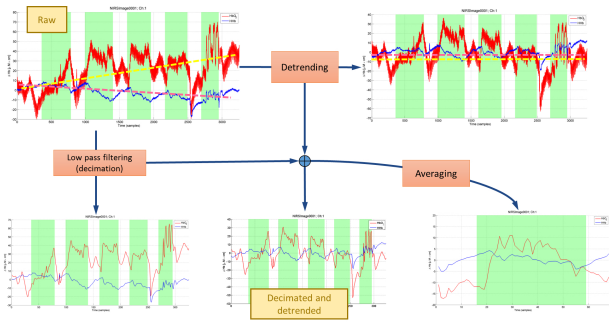

Figure 7: A typical fNIRS processing sequence. Literature is abundant on more aggressive signal processing for fNIRS data, but moderation on the signal processing is advisable as every processing transformation involves assumptions and compromises that should be accounted for during interpretation.

A processing transformation that deserves special attention is registration. Registration, alignment or projection of functional neuroimages over the brain anatomy allows accurately establishing the brain region where brain activity is occurring [129]. The registration operation is central to functional neuroimage analysis permitting the comparison of activity across a cohort of different individuals or longitudinal expressions among others. fNIRS lack a structural counterpart and has to look for alternative solutions; whether projecting to a structural image acquired with other modality, mostly structural magnetic resonance imaging [130], assuming standard positions which probabilistically project over a given cortical location [129] or with virtual projections [131].

The second level of analysis is the ambiguously called analysis itself where the transformation codomain does not match the input domain. Further, when the term pre-processing is used, this level is often referred to as processing. This second level transformation of the information extracts descriptors from the neuroimage. The output might still be confined to a tensor of the same size of the input, however this output is not an enhanced version of the input but distinctly represent different information whereby the semantics of the information has been altered. Common generic neuroimage analysis operations include descriptive statistics, blind source separation including factor analysis, principal component analysis [132] or independent component analysis [133], manifold learning and embedding approaches [134] and transforms such as Fourier [135], or wavelets [136, 137] among others, all of which have been used in fNIRS. In fNIRS, analysis is often targeted at revealing segregational or integrational activity. Associative descriptors are expressed in terms of (regressive) relations with neuroscientific variables of interest. Analysis approaches can be coarsely split into hypothesis-driven or data-driven depending on whether the hypothesis (model) is imposed a priori or a posteriori. Common operations to decode activity include regressions, most times in the form of the general linear model (GLM) [138, 139], correlations [122], frequency coherence [140] and wavelet coherence [137], statistical inference [141] among others. The GLM is described in Eq 8, where $y^{\theta_{k,x}} \in \mathbb{R}^N$ are temporal samples, $\epsilon^{\theta_{k,x}} \in \mathbb{R}^N$ denotes the noise, $X \in \mathbb{R}^{NxM}$ is the design matrix and $\beta^{\theta_{k,x}} \in \mathbb{R}^M$ is the response signal strength.

$$y^{\theta_{k,x}} = X\beta^{\theta_{k,x}} + \epsilon^{\theta_{k,x}} \tag{8}$$

In neuroimages, the GLM based statistical parametric mapping (SPM), originally developed by Friston [142] and later imported to fNIRS [143, 138], has reached a status of de facto gold standard for segregational analysis, but the classical "task minus baseline" approach remains popular [144]. This later can be summarised in a channel-wise matrix of activity (see Figure 8). These two analysis provide concurrent, but not equal, estimation about the underlying brain activity as exemplified in [145]. An excellent review on the analysis of fNIRS can be found in [141]. For integrational analysis, graph theory is becoming highly popular for functional connectivity in neuroimages [18, 146] and has also been used in fNIRS [147], whereas dynamic causal modelling [148] is quickly surpassing structural equa-

tion modelling [149] as the most common choice for understanding effective connectivity in neuroimaging [39], and similarly an fNIRS version has already been developed [144]. Emerging alternatives to these models are topological techniques, based on manifold learning [134] or Bayesian approaches [150, 151, 152]. The analysis operation is not necessarily applied along one dimension (temporal, spatial or signal) at a time, but interestingly across two of them or all of them at once. A variety of software is now freely available for fNIRS neuroimages processing [143, 153, 126] and analysis [143, 138, 154].

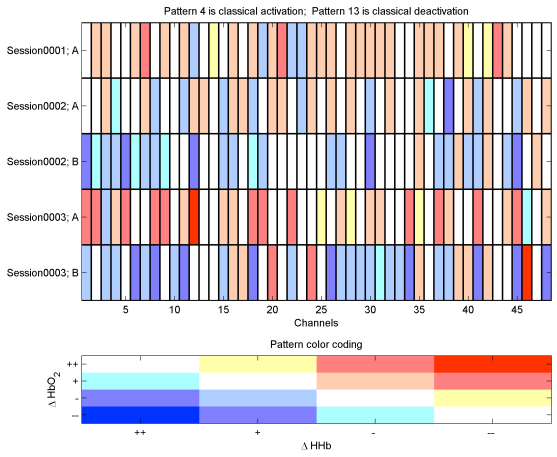

Figure 8: A matrix of channel-wise activity obtained during analysis (generated with software tool ICNA [154]). The activity matrix provides an statistical comparison between values observed during task periods against values observed during baseline periods. Rows represent experimental sessions and conditions and columns represent individual channels. Color indicates statistical significance (++/--) or trend (+/-) of the behaviour of both hemoglobins.

Finally, interpretation of the neuroimage is presented in the languaje of the expert analysing the image. Ideally interpretation of functional neuroimaging are meant to produce models explaining functional processes [155, 148, 156, 157]. This task proves dificult because true causal modelling imposes many challenges still unresolved [158]. Furthermore, interpretation is confined to all the assumptions and/or constraints used in the brain activity reconstruction process. This includes all those from the statistically rigorous formalization of experiment design process and data harvesting [159, 160], the administration of stimulations (block or event related), image formation and reconstruction, as well as those arising from the previous processing and analysis steps. A fundamental element of this puzzle is the model of response function. The response function is a mathematical description of the expected neuroimaging signal spatiotemporal distribution following stimulation. For other neuroimaging modalities it may represent an idealization of the action potential. For fNIRS it takes the form of an hemodynamic response function [35, 161, 139, 137] that is sometimes convolved with the neural kernel [144]. This hemodynamic response function is known to be non-linear [162] and varies with age [163]. Any extrapolation beyond the boundaries imposed by these assumptions and constraints lacks scientific foundation. Moreover, any inference about neuronal activity has to be circumscribed to the specific localization of such activity, inherently affected by partial volume effects [90]. Interpretation benefits from residual analysis and explicit mention of confidence intervals. In other scientific domains, knowledge representation tools [164, 165] such as knowledge discovery and data mining [166], ontologies [167], or semantic networks [167] can fully or partially support and/or autoimatize the process of interpretation, but thus far we are not aware of these tools having yet been used for fNIRS interpretation, except perhaps for timid uses of machine learning precursors of data mining [168].

6. Conclusions

Current neurosciences are unthinkable without the overwhelming contribution of neuroimages. Among whci we found diffuse optics neuroimages with particular interest in the functional subset techniques. Functional images are essential to understand the brain *in-vivo*. We have briefly covered the metabolic activity and the associated neurovascular phenomenon ultimately responsible for the fNIRS signal. We have accompanied the radiation in its travel through the tissues of the human head until its destination in the sensors responsible for image acquisition. We commented several common options for the sampling and quantization of the analog information, and we presented several well-known alternatives for approximating the radiation transport problem. Then we have moved to the reconstruction where the histophysiological information of interest is retrieved. Here, we have commented on the major issues of the ill-possessedness of the problem and the effect of metamerism and how regularization may alleviate the implications. We further presented which is perhaps the most common reconstruction in fNIRS; the direct inversion of the MBLL. Finally, we reached the analysis and discussed some common computational and statistical transformations arriving to the generation of new knowledge regarding brain function. In this stage,

approaches are more diverse all with different implications. We attempted to give an overview of different tools, but we put particular attention to the GLM which can express many experimental designs.

In this journey, many factors either imposed by nature or by the inherent limitation of the models and systems built by humans interfere with this generation of knowledge. Every assumption made has consequences. Table 1 summarizes some important assumptions made in each stage and their corresponding effects. Many factors such as habituation have been intentionally forgotten in this overview for the sake of simplicity. These may demand specific analytical strategies or constrains interpretation but do not necessarily add new steps in the roadmap to interpretation.

Any attempt to understand the function of the brain from diffuse optical neuroimages requires profound knowledge of the brain anatomy, histology and physiology, knowledge regarding its organizational principles and the physico-chemical rules governing such expression of activity, knowledge regarding the physics of image formation and acquisition and the mathematics of image reconstruction, as well as knowledge about the computational and statistical implications of the decisions made during the experiment design and subsequent analysis.

7. Acknowledgments

Funding for this work was provided by projects CONACYT CB-2014-01-237251 and CB-2011-01-169558. JHV was supported by the scholarship CONACYT - 377670.

References

[1] S. Ogawa, T. M. Lee, A. R. Kay, D. W. Tank, Brain magnetic resonance imaging with contrast dependent on blood oxygenation, Proceedings of the National Academy of Sciences 87 (1990) 9868–9872.

[2] E. Macé, G. Montaldo, I. Cohen, M. Baulac, M. Fink, M. Tanter, Functional ultrasound imaging of the brain, Nature Methods 8 (2011) 662?664.

[3] K. Deisseroth, Optogenetics, Nature methods 8 (1) (2011) 26–29.

[4] K. Chung, K. Deisseroth, Clarity for mapping the nervous system, Nature methods 10 (6) (2013) 508–513.

[5] E. Mace, J. Orange, Visualization of the immunological synapse by dual color time-gated stimulated emission depletion (sted) nanoscopy, J Vis Exp. 85.

[6] D. A. Boas, A. M. Dale, M. A. Franceschini, Diffuse optical imaging of brain activation: Approaches to optimizing image sensitivity, resolution and accuracy, NeuroImage 23 (2004) S275–S288.

[7] F. F. J?bsis, Noninvasive, infrared monitoring of cerebral and myocardial oxygen sufficiency and circulatory parameters, Science, New Series 198 (4323) (1977) 1264–1267.

[8] G. Strangman, D. A. Boas, J. P. Sutton, Non-invasive neuroimaging using near-infrared light, Biological Psychiatry 52 (2002) 679–693.

[9] M. Ferrari, L. Mottola, V. Quaresima, Principles, techniques, and limitations of near infrared spectroscopy, Canadian Journal of Applied Physiology 29 (4) (2004) 463–487.

[10] M. Ferrari, V. Quaresima, A brief review on the history of human functional near-infrared spectroscopy (fNIRS) development and fields of application, Neuroimage 63 (2012) 921–935.

[11] Y. Hoshi, Functional near-infrared spectroscopy: current status and future prospects, Journal of Biomedical Optics 12 (6) (2007) 062106.

[12] Y. Hoshi, M. Shimada, C. Sato, Y. Iguchi, Reevaluation of near-infrared light propagation in the adult human head: implications for functional near-infrared spectroscopy, Journal of Biomedical Optics 10 (6) (2005) 064032.

[13] F. Scholkmann, S. Kleiser, A. J. Metz, R. Zimmermann, J. M. Pavia, U. Wolf, M. Wolf, A review on continuous wave functional near-infrared spectroscopy and imaging instrumentation and methodology, Neuroimage 85 (2014) 6–27.

[14] A. Villringer, B. Chance, Non-invasive optical spectroscopy and imaging of human brain function, Trends in Neuroscience 20 (10) (1997) 435–442.

[15] D. A. Boas, C. Pitris, N. Ramanujam (Eds.), Handbook of Biomedical Optics, CRC Press, 2011.

[16] M. F. Bear, B. W. Connors, M. A. Paradiso, Neuroscience: Exploring the brain, 3rd Edition, Lippincott Williams and Wilkins, 2006.

[17] L. Squire, D. Berg, F. Bloom, S. du Lac, A. Ghosh, N. Spitzer, Fundamental Neuroscience, 3rd Edition, Elsevier Academic Press, 2008.

[18] E. Bullmore, O. Sporns, Complex brain networks: graph theoretical analysis of structural and functional systems., Nature Reviews Neuroscience 10(3).

[19] F. A. C. Azevedo, L. R. B. Carvalho, L. T. Grinberg, J. M. Farfel, R. E. L. Ferretti, R. E. P. Leite, W. J. Filho, R. Lent, S. Herculano-Houzel, Equal numbers of neuronal and nonneuronal cells make the human brain an isometrically scaled-up primate brain, Journal of Comparative Neurology 513 (2009) 532–541.

[20] M. F. Glasser, T. S. Coalson, E. C. Robinson, C. D. Hacker, J. Harwell, E. Yacoub, K. Ugurbil, J. Andersson, C. F. Beckmann, M. Jenkinson, S. M. Smith, D. C. van Hessen, A multimodal parcellation of human cerebral cortex, Nature E-pub ahead of print (2016) 10 pp.

[21] R. Carter, The human brain book, 2nd Edition, KD, 2014.

[22] E. R. Kandel, J. H. Schwartz, T. M. Jessel, S. A. Siegelbaum, A. J. Hudspeth, Principles of Neural Science, 5th Edition, McGraw-Hill Professional, 2012.

[23] J. R. Fallon, A. B. Taylor, Protein Synthesis in Neurons, John Wiley & Sons, 2006.

[24] E. Armstrong, Relative brain size and metabolism in mammals, Science 220 (1983) 1302?1304.

[25] P. Mitchell, Coupling of phosphorylation to electron and hydrogen transfer by a chemi-osmotic type of mechanism, Nature 191 (1961) 144?148.

[26] A. Gjedde, Handbook of Neurochemistry and Molecular Neurobiology. Brain Energetics. Integration of Molecular and Cellular Processes, Springer, 2007, Ch. Chapter 4.4. Coupling of Brain Function to Metabolism: Evaluation of Energy Requirements, pp. 343–400.

[27] M. A. Mintun, B. N. Lundstrom, A. Z. Snyder, A. G. Vlassenko, G. L. Shulman, M. E. Raichle, Blood flow and oxygen delivery to human brain during functional activity: Theoretical modeling and experimental data, Proceedings of the National Academy of Sciences 98 (12) (2001) 6859–6864.

[28] P. L. Nunez, R. Srinivasan, Electric fields of the brain: the neurophysics of EEG, 2nd Edition, Oxford University Press, 2006.

[29] A. A. Grace, B. S. Bunney, Intracellular and extracellular electrophysiology of a nigral dopaminergic neurons - 2. action potential generating mechanisms and morphological correlates, Neuroscience 10 (2) (1983) 317–331.

[30] R. H. Garman, Histology of the central nervous system, Toxicologic Pathology 39 (2011) 22–35.

[31] M. A. Franceschini, D. A. Boas, Noninvasive measurement of neuronal activity with near-infrared optical imaging, NeuroImage 21 (2004) 372–386.

[32] S. A. Sheth, M. Nemoto, M. W. Guiou, M. A. Walker, N. Pouratian, A. W. Toga, Linear and nonlinear relationships between neuronal acivity, oxygen metabolism and hemodynamic responses, Neuron 42 (2004) 347–355.

[33] S. A. Sheth, M. Nemoto, M. W. Guiou, M. A. Walker, A. W. Toga, Spatiotemporal evolution of functional hemodynamic changes and their relationship to neuronal activity, Journal of Cerebral Blood Flow and Metabolism 25 (2005) 830–841.

[34] R. B. Buxton, K. Uludag, D. J. Dubowitz, T. T. Liu, Modeling the hemodynamic response to brain activation, NeuroImage 23 (2004) S220–S233.

[35] S. G. Diamond, T. J. Huppert, V. Kolehmainen, M. A. Franceschini, J. P. Kaipio, S. R. Arridge, D. A. Boas, Dynamic physiological modelling for functional diffuse optical tomography, NeuroImage 30 (2006) 88–101.

[36] R. S. J. Frackowiak, K. J. Friston, C. D. Frith, R. J. Dolan, C. J. Price, S. Zeki, J. Ashburner, W. Penny, Human brain function, 2nd Edition, Elsevier Academic Press, 2004.

[37] B. Horwitz, The elusive concept of brain connectivity, NeuroImage 19 (2003) 466–470.

[38] P. Hagmann, L. Jonasson, P. Maeder, J.-P. Thiran, V. J. Wedeen, R. Meuli, Understanding diffusion MR imaging techniques: from scalar Diffusion-Weighted imaging to Diffusion Tensor imaging and beyond, RadioGraphics 26 (2006) S205–S223.

[39] K. J. Friston, Functional and effective connectivity: a review, Brain connectivity 1 (1) (2011) 13–36.

[40] P. R. Huttenlocher, Neural plasticity, Harvard University Press, 2009.

[41] J. M. Park, S.-C. Jung, S.-Y. Eun, Long-term synaptic plasticity: circuit perturbation and stabilization, Korean Journal of Physiology and Pharmacology 18 (2014) 457–460.

[42] E. Gratton, V. Toronov, U. Wolf, M. Wolf, A. Webb, Measurement of brain activity by near-infrared light, Journal of Biomedical Optics 10 (1) (2005) 011008.

[43] A. V. Medvedev, J. Kainerstorfer, S. V. Borisov, R. L. Barbour, J. VanMeter, Event-related fast optical signal in a rapid object recognition task: Improving detection by the independent component analysis, Brain Research 1236 (2008) 145–148.

[44] J. Steinbrink, F. C. D. Kempf, A. Villringer, H. Obrig, The fast optical signal?robust or elusive when non-invasively measured in the human adult?, NeuroImage 26 (2005) 996–1008.

[45] M. Wolf, U. Wolf, J. H. Choi, R. Gupta, L. P. Safonova, L. A. Paunescu, A. Michalos, E. Gratton, Functional frequency-domain near-infrared spectroscopy detects fast neuronal signal in the motor cortex, NeuroImage 17 (2002) 1868–1875.

[46] C. E. Elwell, H. Owen-Reece, M. Cope, A. D. Edwards, J. S. Wyatt, E. O. R. Reynolds, D. T. Delpy, Measurement of changes in cerebral haemodynamics during inspiration and expiration using near infrared spectroscopy, Advances in Experimental Medicine and Biology 345 (1994) 619–626.

[47] C. E. Elwell, R. Springett, E. M. C. Hillman, D. T. Delpy, Oscillations in cerebral haemodynamics - implications for functional activation studies, Advances in Experimental Medicine and Biology 471 (1999) 57–65.

[48] M. A. Franceschini, S. Fantini, J. H. Thompson, J. P. Culver, D. A. Boas, Hemodynamic evoked response of the sensorimotor cortex measured noninvasively with near-infrared optical imaging, Psychophysiology 40 (2003) 548–560.

[49] J. H. Meek, C. E. Elwell, M. J. Khan, J. Romaya, J. S. Wyatt, D. T. Delpy, S. Zeki, Regional changes in cerebral haemodynamics as a result of a visual stimulus measured by near infrared spectroscopy, Proceedings of the Royal Society: Biological Sciences 261 (1362) (1995) 351–356.

[50] M. A. Franceschini, D. K. Joseph, T. J. Huppert, S. G. Diamond, D. A. Boas, Diffuse optical imaging of the whole head, Journal of Biomedical Optics 11 (5) (2006) 054007.

[51] E. Kirilina, N. Yu, A. Jelzow, H. Wabnitz, A. M. Jacobs, I. Tachtsidis, Identifying and quantifying main components of physiological noise in functional near infrared spectroscopy on the prefrontal cortex, Frontiers in Human Neuroscience 7 (2013) 864 (17pp).

[52] I. Tachtsidis, F. Scholkmann, False positives and false negatives in functional near-infrared spectroscopy: issues, challenges, and the way forward, Neurophotonics 3 (3) (2016) 030401.

[53] D. R. Leff, F. Orihuela-Espina, T. Athanasiou, V. Karimyan, C. E. Elwell, A. W. Darzi, G.-Z. Yang, Circadian cortical compensation: a longitudinal fNIRS study of sleep deprivation in surgical trainees, Annals of Surgery 252 (6) (2009) 1082–1090.

[54] S. G. Diamond, K. L. Perdue, D. A. Boas, A cerebrovascular response model for functional neuroimaging including dynamic cerebral autoregulation, Mathematical Biosciences 220 (2009) 102–117.

[55] S. L. Jacques, B. W. Pogue, Tutorial on diffuse light transport, Journal of Biomedical Optics 13 (4) (2008) 041302.

[56] P. Rolfe, In vivo near infrared spectroscopy, Annual Review of Biomedical Engineering 2 (2000) 715–754.

[57] R. B. Bird, W. E. Stewart, E. N. Lightfoot, Transport phenomena, 2nd Edition, John Wiley & Sons, 2006.

[58] R. H. Webb, Elementary Wave Optics, Dover Books on Physics, Dover Publications, 2005.

[59] E. Claridge, S. Cotton, P. Hall, M. Moncrieff, From colour to tissue histology: Physics-based interpretation of images of pigmented skin lesions, Medical Image Analysis 7 (2003) 489–502.

[60] J. C. Hebden, S. R. Arridge, D. T. Delpy, Optical imaging in medicine: I. experimental techniques, Physics in Medicine and Biology 42 (1997) 825–840.

[61] J. B. Pawley, Handbook Of Biological Confocal Microscopy, 3rd Edition, Springer-Verlag, 2006, Ch. Chapter 4. Points, pixels and gray levels: digitizing image data, pp. 59–79.

[62] F. Orihuela-Espina, D. R. Leff, D. R. C. James, A. W. Darzi, G.-Z. Yang, Quality control and assurance in functional near infrared spectroscopy (fNIRS) experimentation, Physics in Medicine and Biology 55 (2010) 3701–3724.

[63] Q. Li, X. He, Y. Wang, H. Liu, D. Xu, F. Guo, Review of spectral imaging technology in biomedical engineering: achievements and challenges, Journal of Biomedical Optics 18 (10) (2013) 100901.

[64] Z. Zalevsky, Defying abbe?s law, Nature Photonics 7 (2013) 593–594.

[65] M. Senoner, T. Wirth, W. E. S. Unger, Imaging surface

analysis: Lateral resolution and its relation to contrast and noise, Journal of Analytical Atomic Spectrometry 25 (2010) 1440?1452.

[66] M. Essenpreis, C. E. Elwell, M. Cope, P. Zee van der, S. R. Arridge, D. T. Delpy, Spectral dependence of temporal point spread functions in human tissues, Applied Optics 32 (4) (1993) 418–425.

[67] A. T. Eggebrecht, S. L. Ferradal, A. Robichaux-Viehoever, M. S. Hassanpour, H. Dehghani, A. Z. Snyder, T. Hershey, J. P. Culver, Mapping distributed brain function and networks with diffuse optical tomography, Nature Photonics 8 (2014) 484–454.

[68] Y. Ito, R. P. Kennan, E. Watanabe, H. Koizumi, Assessment of heating effects in skin during continuous wave infrared spectroscopy, Journal of Biomedical Optics 5 (4) (2000) 383–390.

[69] M. Wolf, M. Ferrari, V. Quaresima, Progress of near-infrared spectroscopy and topography for brain and muscle clinical applications, Journal of Biomedical Optics 12 (6) (2007) 062104.

[70] P. Phan, D. Highton, I. Tachtsidis, M. Smith, C. Elwell, A new multichannel broadband near infrared spectroscopy system to measure the spatial distribution od cytochrome-c-oxydase and tissue oxygenation, in: OSA Biomedical Optics (BIOMED) meeting, 2016, p. 5 pp.

[71] R. Saager, A. Berger, Measurement of layer-like hemodynamic trends in scalp and cortex: implications for physiological baseline suppresion in functional near-infrared spectroscopy, Journal of Biomedical Optics 13 (3) (2008) 034017.

[72] P. P. C. A. F. L. S. P. E. S. A. M. A. H. S. G. P. B. I. Tachtsidis, Real-world neuroimaging: the use of a fiberless and wearable fnirs system to monitor brain activity in the real-life on freely moving participants, in: Biannual Metting of the Society for functional Near Infrared Spectroscopy, Université Paris Descartes, 12 rue de l'Ecole de Médecine, Paris, 2016.

[73] R. E. Thilwind, G. Hooft, N. E. Uzunbajakava, Improved depth resolution in near-infrared diffuse reflectance spectroscopy using obliquely oriented fibers, Journal of Biomedical Optics 14 (2) (2009) 024026.

[74] H. Sato, N. Tanaka, M. Uchida, Y. Hirabayashi, M. Kanai, T. Ashida, I. Konishi, A. Maki, Wavelet analysis for detecting body movement artifacts in optical topography signals, NeuroImage 33 (2006) 580–587.

[75] Y. Dancik, A. Favre, C. J. Loy, A. V. Zvyagin, M. S. Roberts, Use of multiphoton tomography and fluorescence lifetime imaging to investigate skin pigmentation in vivo, Journal of Biomedical Optics 18 (2) (2013) 026022.

[76] Y. Yamashita, A. Maki, H. Koizumi, Wavelength dependence of the precision of non-invasive optical measurement of oxy-, deoxy- and total-hemoglobin concentration, Medical Physics 28 (6) (2001) 1108–1114.

[77] H. Sato, M. Kiguchi, A. Maki, Wavelength dependence of effective pathlength factor in noninvasive optical measurements of human brain functions, Japanese Journal of Applied Physics 45 (12) (2006) L361–L363.

[78] H. Sato, M. Kiguchi, F. Kawaguchi, A. Maki, Practicality of wavelength selection to improve signal-to-noise ratio in near-infrared spectroscopy, NeuroImage 21 (2004) 1554–1562.

[79] G. Gratton, C. R. Brumback, B. A. Gordon, M. A. Pearson, K. A. Low, M. Fabiani, Effects of measurement method, wavelength, and source-detector distance on the fast optical signal, NeuroImage 32 (2006) 1576–1590.

[80] I. Tachtsidis, T. S. Leung, L. Devoto, D. T. Delpy, C. E. Elwell, Measurement of frontal lobe functional activation and related systemic effects: a near infrared spectroscopy investigation, Advances in Experimental Medicine and Biology 614 (2008) 397–403.

[81] I. Tachtsidis, T. S. Leung, A. Chopra, P. H. Koh, C. B. Reid, C. E. Elwell, False positives in functional near infrared topography, Advances in Experimental Medicine and Biology 645 (2009) 307–314.

[82] T. Katura, N. Tanaka, A. Obata, H. Sato, A. Maki, Quantitative evaluation of interrelations between spontaneous low-frequency oscillations in cerebral hemodynamics and systemic cardiovascular dynamics, NeuroImage 31 (2006) 1592–1600.

[83] Q. Zhang, E. N. Brown, G. E. Strangman, Adaptive filtering for global interference cancellation and real-time recovery of evoked brain activity: a monte carlo simulation study, Journal of Biomedical Optics 12 (4) (2007) 044014.

[84] Q. Zhao, L. Ji, T. Jiang, Improving depth resolution of diffuse optical tomography with a layer-based sigmoid adjustment method, Optics Express 15 (7) (2007) 4018–4029.

[85] M. Kohl-Bareis, H. Obrig, J. Steinbrink, J. Malak, K. Uludag, A. Villringer, Noninvasive monitoring of cerebral blood flow by dye bolus method: Separation of brain from skin and skull signals, Journal of Biomedical Optics 7 (3) (2002) 464–470.

[86] D. A. Boas, K. Chen, D. Grebert, M. A. Franceschini, Improving the diffuse optical imaging spatial resolution of the cerebral hemodynamic response to brain activation in humans, Optics Letters 29 (13) (2004) 1506–1508.

[87] M. W. Hemelt, K. Kang, Determination of a biological absorber depth utilizing multiple source-detector spearations and multiple frequency values of near-infrared time-resolved spectroscopy, Biotechnology progress 15 (4) (1999) 622–629.

[88] T. Yamamoto, A. Maki, T. Kadoya, Y. Tanikawa, Y. Yamada, E. Okada, H. Koizumi, Arranging optical fibers for the spatial resolution improvement of topographical images, Physics in Medicine and Biology 47 (2002) 3429–3440.

[89] D. A. Boas, G. Strangman, J. P. Culver, R. D. Hoge, G. Jasdzewski, R. A. Poldrack, B. R. Rosen, J. B. Mandeville, Can the cerebral metabolic rate of oxygen be estimated with near-infrared spectroscopy?, Physics in Medicine and Biology 48 (2003) 2405–2418.

[90] J. Dukart, A. Bertolino, When structure affects function - the need for partial volume effect correction in functional and resting state magnetic resonance imaging studies, PLoS One 9 (12) (2014) e114227.

[91] A. Maki, Y. Yamashita, Y. Ito, E. Watanabe, Y. Mayanagi, H. Koizumi, Spatial and temporal analysis of human motor activity using non-invasive nir topography, Medical Physics 22 (12) (1995) 1997–2005, the temporal analysis is actually static samples snapshots at different times...

[92] J. P. Culver, B. L. Schlaggar, H. Dehghani, B. W. Zeff, Diffuse optical tomography for mapping human brain function, in: IEEE/NLM Life Science Systems and Applications workshop (LSSA'06), IEEE, 2006, pp. 1–2.

[93] V. Ntziachristos, J. Ripoll, L. V. Wang, R. Weissleder, Looking and listening to light: the evolution of whole-body photonic imaging, Nature biotechnology 23 (3) (2005) 313–320.

[94] A. Torricelli, D. Contini, A. Pifferi, M. Caffini, R. Re, L. Zucchelli, L. Spinelli, Time domain functional nirs imaging for human brain mapping, Neuroimage 85 (2014) 28–50.

[95] G. Yu, T. Durduran, C. Zhou, R. Cheng, A. G. Yodh, Handbook of Biomedical Optics, CRC Press, 2011, Ch. Near-infrared diffuse correlation spectroscopy for assessment of tissue blood flow (Ch.10), pp. 195–216.

[96] Q. Fang, D. A. Boas, Monte carlo simulation of photon migration in 3D turbid media accelerated by graphics processing units, Optics Expr 17 (22) (2009) 20178–20190.

[97] B. Cuervo-Soto, J. Herrera-Vega, J. A. del C. Garcés-Báez, C. T. no Palacios, F. Orihuela-Espina, Mocarts: A lightweight radiation transport simulator for easy handling of complex

sensing geometries, in: 13th International Symposium on Biomedical Imaging (ISBI'16), 2016, pp. 377–380.

[98] C. Chuang, C. Chen, Y. Hsieh, T. Liu, C. Sun, Brain structure and spatial sensitivity profile assessing by near-infrared spectroscopy modeling based on 3D MRI data, Journal of Biophotonics 6 (3) (2013) 267–274.

[99] M. Cope, D. T. Delpy, E. O. R. Reynolds, S. Wray, J. S. Wyatt, P. Zee van der, Methods of quantitating cerebral near infrared spectroscopy data, Advances in Experimental Medicine and Biology 222 (1988) 183–189.

[100] D. T. Delpy, M. Cope, P. Zee van der, S. R. Arridge, S. Wray, J. S. Wyatt, Estimation of optical pathlength through tissue from direct time of flight measurement, Physics in Medicine and Biology 33 (12) (1988) 1433–1442.

[101] A. Sassaroli, S. Fantini, Comment on the modified beer-lambert law, Physics in Medicine and Biology 49 (2004) N255–N257.

[102] D. Haensse, P. Szabo, D. Brown, J.-C. Fauch??re, P. Niederer, H.-U. Bucher, M. Wolf, New multichannel near-infrared spectrophotometry system for functional studies of the brain in adults and neonates, Optics Express 13 (12) (2005) 4525–4538.

[103] P. Zee van der, M. Cope, S. R. Arridge, M. Essenpreis, L. A. Potter, A. D. Edwards, J. S. Wyatt, D. C. McCormick, S. C. Roth, E. O. R. Reynolds, D. T. Delpy, Experimentally measured optical pathlength for the adult head, calf and forearm and the head of the newborn infant as a function of inter optode spacing, Advances in Experimental Medicine and Biology 316 (1992) 143–153.

[104] S. R. Arridge, J. C. Hebden, D. T. Delpy, Optical imaging in medicine: Ii. modelling and reconstruction, Physics in Medicine and Biology 42 (1997) 841–853.

[105] H. Dehghani, S. Srinivasan, B. W. Pogue, A. P. Gibson, Numerical modelling and image reconstruction in diffuse optical tomography, Philosophical Transactions of the Royal Society of London. Serie A 367 (2009) 3073–3093.

[106] S. J. Preece, E. Claridge, Spectral filter optimization for the recovery of parameters which describe human skin, IEEE Transactions on Pattern Analysis and Machine Intelligence 26 (7) (2004) 1–10.

[107] M. Kimiyoshi, N. Tsumura, Application of image quality metamerism to investigate gold color area in cultural property, Journal of Electronic Imaging 22 (1) (2013) 013029.

[108] H. Engl, M. Hanke, A. Neubauer, Regularization of Inverse Problems, Springer Science & Business Media, 1996.

[109] A. Neumaier, Solving ill-conditioned and singular linear systems: A tutorial on regularization, SIAM review (1998) 32 pp.

[110] A. Tikhonov, Numerical Methods for the Solution of Ill-Posed Problems, Springer Science & Business Media, 1995.

[111] Y. Zhan, A. T. Eggebrecht, J. P. Culver, H. Dehghani, Image quality analysis of high density diffuse optical tomography incorporating a subject-specific head model, Frontiers in Neuroenergetics 4 (2012) 6 (9pp).

[112] X. Wu, A. T. Eggebrecht, S. L. Ferradal, J. P. Culver, H. Dehghani, Fast and efficient image reconstruction for high density diffuse optical imaging of the human brain, Biomedical Optics Express 6 (11) (2015) 4567–4584.

[113] T. Tarvainen, V. Kolehmainen, M. Vauhkonen, A. Vanne, A. P. Gibson, M. Schweiger, S. R. Arridge, J. P. Kaipio, Computational calibration method for optical tomography, Applied Optics 44 (10) (2005) 1879–1888.

[114] S. Oh, A. B. Milstein, R. P. Millane, C. A. Bouman, J. Webb, Kevin, Source-detector calibration in three-dimensional bayesian optical diffusion tomography, Journal of the Optical Society of America A 19 (10) (2005) 1983–1993.

[115] I. Nissilä, T. Noponen, K. Kotilahti, T. Katila, L. Lipi??inen, T. Tarvainen, M. Schweiger, S. R. Arridge, Instrumentation and calibration methods for the multichannel measurement of phase and amplitude in optical tomography, Review of Scientific Instruments 76 (2005) 044302.

[116] L. Kocsis, P. Herman, A. Eke, The modified beer-lambert law revisited, Physics in Medicine and Biology 51 (2006) N91–N89.

[117] K. Uludag, M. Kohl, J. Steinbrink, H. Obrig, A. Villringer, Cross talk in the Lambert-Beer calculation for near-infrared wavelengths estimated by Monte Carlo simulations, Journal of Biomedical Optics 7 (1) (2002) 51–59.

[118] K. Uludag, J. Steinbrink, A. Villringer, H. Obrig, Separability and cross-talk: optimizing dual wavelength combinations for near-infrared spectroscopy of the adult head, NeuroImage 22 (2004) 583–589.

[119] D. Arifler, T. Zhu, S. Madaan, I. Tachtsidis, Optimal wavelength combinations for near-infrared spectroscopic monitoring of changes in brain tissue hemoglobin and cytochrome c oxidase concentrations, Biomedical Optics Express 6 (3) (2015) 933–947.

[120] H. Dehghani, B. R. White, B. W. Zeff, A. Tizzard, J. P. Culver, Depth sensitivity and image reconstruction analysis of dense imaging arrays for mapping brain function with diffuse optical tomography, Applied Optics 48 (10) (2009) D137–D143.

[121] N. Lange, S. L. Zeger, Non-linear fourier time series analysis for human brain mapping by functional magnetic resonance imaging, Applied Statistics 46 (1) (1997) 1–29.

[122] X. Cui, S. Bray, A. L. Reiss, Functional near infrared spectroscopy (nirs) signal improvement based on negative correlation between oxygenated and deoxygenated hemoglobin dynamics, NeuroImage 49 (2010) 3039–3046.

[123] M. Pe?a, A. Maki, D. Kovaci??, G. Dehaene-Lambertz, H. Koizumi, F. Bouquet, J. Mehler, Sounds and silence: an optical topography study of language recognition at birth, Proceedings of the National Academy of Sciences 100 (20) (2003) 11702–11705.

[124] F. C. Robertson, T. S. Douglas, E. M. Meintjes, Motion artefact removal for functional near infrared spectroscopy: a comparison of methods, IEEE Transactions on Biomedical Engineering Epub ahead of print.

[125] F. Scholkmann, S. Spichtig, T. Muehlemann, M. Wolf, How to detect and reduce movement artifacts in near-infrared imaging using moving standard deviation and spline interpolation, Physiological measurement 31 (5) (2010) 649.

[126] T. J. Huppert, S. G. Diamond, M. A. Franceschini, D. A. Boas, Homer: a review of time-series analysis methods for near-infrared spectroscopy of the brain, Applied Optics 48 (10) (2009) D280–D298.

[127] S. Sanei, J. A. Chambers, EEG signal processing, John Wiley & Sons, 2007.

[128] V. Toronov, M. A. Franceschini, M. Filiaci, S. Fantini, M. Wolf, A. Michalos, E. Gratton, Near-infrared study of fluctuations in cerebral hemodynamics during rest and motor stimulation: Temporal analysis and spatial mapping, Medical Physics 27 (4) (2000) 801–815.

[129] M. Okamoto, H. Dan, K. Sakamoto, K. Takeo, K. Shimizu, S. Kohno, I. Oda, S. Isobe, T. Suzuki, K. Kohyama, I. Dan, Three-dimensional probabilistic anatomical cranio-cerebral correlation via the international 10-20 system oriented for transcranial functional brain mapping, NeuroImage 21 (2004) 99–111.

[130] H. Ayaz, M. Izzetoglu, S. M. Platek, S. Bunce, K. Izzetoglu, K. Pourrezaei, B. Onaral, Registering fnir data to brain surface image using mri templates, in: Proceedings of the 28th IEEE

EMBS Annual International Conference, 2006.
[131] D. Tsuzuki, V. Jurcak, A. K. Singh, M. Okamoto, E. Watanabe, I. Dan, Virtual spatial registration of stand-alone fnirs data to mni space, Neuroimage 34.
[132] Y. Zhang, D. H. Brooks, M. A. Franceschini, D. A. Boas, Eigenvector-based spatial filtering for reduction of physiological interference in diffuse optical imaging, Journal of Biomedical Optics 10 (1) (2005) 011014.
[133] C. B. Akgül, A. Akin, B. Sankur, Extraction of cognitive activity-related waveforms from functional near-infrared spectroscopy signals, Medical and Biological Engineering and Computing 44 (2006) 945–958.
[134] D. R. Leff, F. Orihuela-Espina, L. Atallah, A. W. Darzi, G.-Z. Yang, Functional near infrared spectroscopy in novice and expert surgeons: a manifold embedding approach, in: N. Ayache, S. Ourselin, A. Maeder (Eds.), Medical Image Computing and Computer-Assisted Intervention (MICCAI'07), Vol. 4792, Lecture Notes in Computer Science, Australia, 2007, pp. 270–277.
[135] P. P. Mitra, B. Pesaran, Analysis of dynamic brain imaging data, Biophysical journal 76 (1999) 691–708.
[136] J. M. Lina, M. Dehaes, C. Matteau-Pelletier, F. Lesage, Complex wavelets applied to diffuse optical spectroscopy for brain activity detection, Optics Express 16 (2) (2008) 1029–1050.
[137] X. Zhang, J. Yu, R. Zhao, W. Xu, H. Niu, Y. Zhang, N. Zuo, T. Jiang, Activation detection in functional near-infrared spectroscopy by wavelet coherence, Journal of biomedical optics 20 (1) (2015) 016004.
[138] J. C. Ye, S. Tak, K. E. Jang, J. Jung, J. Jang, Nirs-spm: Statistical parametric mapping for near-infrared spectroscopy, NeuroImage 44 (2009) 428–447.
[139] M. Uga, I. Dan, T. Sano, H. Dan, E. Watanabe, Optimizing the general linear model for functional near-infrared spectroscopy: an adaptive hemodynamic response function approach, Neurophotonics 1 (1) (2014) 015004.
[140] M. L. Schroeter, M. M. B?cheler, K. M?ller, K. Uludag, H. Obrig, G. Lohmann, M. Tittgemeyer, A. Villringer, D. Y. Cramon von, Towards a standard analysis for functional near-infrared imaging, NeuroImage 21 (2004) 283–290.
[141] S. Tak, J. C. Ye, Statistical analysis of fNIRS data: a comprehensive review, NeuroImage 85 (Part 1) (2014) 72–91.
[142] K. J. Friston, A. P. Holmes, K. J. Worsley, J.-B. Poline, C. D. Frith, R. S. J. Frackowiak, Statistical parametric maps in functional imaging: a general linear approach, Human Brain Mapping 2 (1995) 189–210.
[143] P. H. Koh, D. E. Glaser, G. Flandin, S. J. Kiebel, B. Butterworth, A. Maki, D. T. Delpy, C. E. Elwell, Functional optical signal analysis: a software tool for near-infrared spectroscopy data processing incorporating statistical parametric mapping, Journal of Biomedical Optics 12 (6) (2007) 064010.
[144] S. Tak, A. N. Kempny, K. J. Friston, A. P. Leff, W. D. Penny, Dynamic causal modelling for functional near-infrared spectroscopy, Neuroimage 111 (2015) 338–349.
[145] G. Paggetti, D. R. Leff, F. Orihuela-Espina, G. P. Mylonas, A. W. Darzi, G.-Z. Yang, G. Menegaz, The role of the posterior parietal cortex in stereopsis and hand-eye coordination during motor task behaviours, Cognitive Processing In press.
[146] O. Sporns, Networks of the brain, MIT Press, 2011.
[147] D. R. C. James, F. Orihuela-Espina, D. R. Leff, G. P. Mylonas, K.-W. Kwok, A. W. Darzi, G.-Z. Yang, Cognitive burden estimation for visuomotor learning with fNIRS, in: Medical Image Computing and Computer-Assisted Intervention (MICCAI 2010) in Lecture Notes in Computer Science, Vol. 6363, 2010, pp. 319–326.
[148] K. J. Friston, L. Harrison, W. Penny, Dynamic causal modelling, NeuroImage 19 (2003) 1273–1302.
[149] A. R. McIntosh, F. Gonzalez Lima, Structural equation modelling and its application to network analysis in functional brain imaging, Human Brain Mapping 2 (1994) 2–22.
[150] J. C. Rajapakse, J. Zhou, Learning effective brain connectivity with dynamic bayesian networks, Neuroimage 37 (2007) 749–760.
[151] K. Yang, J. C. Rajapakse, An exploratory approach to modelling effective connectivity, in: IEEE International Symposium on Biomedical Imaging: Nano to Macro (ISBI'04), Vol. 1, IEEE, Arlington, VA, USA, 2004, pp. 844– 847.
[152] S. A. Montero-Hernández, F. Orihuela-Espina, J. Herrera-Vega, L. E. Sucar, Causal probabilistic graphical models for decoding effective connectivity in functional near infrared spectroscopy, in: 29th International Florida AI Research Society (FLAIRS) Conference, Miami, Florida, USA, 2016, pp. 686–689.
[153] G. E. Strangman, Q. Zhang, T. Zeffiro, Near-infrared neuroimaging with ninpy, Frontiers in Neuroinformatics 3 (2009) 12 (13 pp.).
[154] F. Orihuela-Espina, D. R. Leff, D. R. C. James, A. W. Darzi, G.-Z. Yang, ICNA: A software tool for manifold embedded based analysis of functional near infrared spectroscopy data, in: 15th Annual meeting of the Organization of Human Brain Mapping (OHBM 2009), San Francisco, CA, USA, 2009.
[155] L. A. Baccalá, K. Sameshima, Partial directed coherence: a new concept in neural structure determination, Biological Cybernetics 84 (2001) 463–474.
[156] M. Kaminski, M. Ding, W. A. Truccolo, S. L. Bressler, Evaluating causal relations in neural systems: Granger causality, directed transfer function and statistical assessment of significance, Biological Cybernetics 85 (2001) 145–157.
[157] J. Pearl, Causal inference in statistics: an overview, Statistics surveys 3 (2009) 96–146.
[158] J. Pearl, Causality: Models, Reasoning and Inference, 2nd Edition, Cambridge University Press, 2009.
[159] G. E. P. Box, W. G. Hunter, J. S. Hunter, W. G. Hunter, Statistics for experimenters: An introduction to design, data analysis and model building, John Wiley & Sons, 1978.
[160] A. Dean, D. Voss, Design and analysis of experiments, Springer Texts in Statistics, Springer, 2000.
[161] Y. Zhang, D. H. Brooks, D. A. Boas, A haemodynamic response function model in spatio-temporal diffuse optical tomography, Physics in Medicine and Biology 50 (2005) 4625–4644.
[162] V. Sharma, G. Kaundinya, R. Parlapalli, R. Briggs, H. Liu, Nonlinearity of hemodynamic response in motor cortex measured by near infrared spectroscopy, in: Biomedical Optics (BIOMED 2008), St. Petersburg, Florida, United States, 2008, p. BMD13.
[163] M. L. Schroeter, S. Zysset, F. Kruggel, D. Y. von Crammon, Age dependency of the haemodynamic response as measured by functional near-infrared spectroscopy, NeuroImage 19 (2003) 555–564.
[164] J. F. Sowa, Knowledge Representation: Logical, Philosophical, and Computational Foundations, Brooks Cole Publishing, 2000.
[165] R. Davis, H. Shrobe, P. Szolovits, What is a knowledge representation?, AI Magazine 14 (1) (1993) 17–33.
[166] U. Fayyad, G. Piatetsky-Shapiro, P. Smyth, From data mining to knowledge discovery in databases, Artificial Intelligence Magazine 17 FALL (3) (1996) 37–54.
[167] D. Gašević, D. Djurić, V. Devedžić, Model driven engineering and ontology development, 2nd Edition, Springer-Verlag, 2009.

[168] S. Fantini, A. Sassaroli, Y. Tong, L. H. Hirshfield, A. Girouard, E. T. Solovey, , R. J. Jacob, Real-time assessment of mental workload with near-infrared spectroscopy: Potential for human-computer interaction, in: Biomedical Optics (BIOMED), St. Petersburg, Florida, United States, 2008, p. BMD14.

[169] M. S. Patterson, B. C. Wilson, D. R. Wyman, The propagation of optical radiation in tissue i. models of radiation transport and their application, Lasers in Medical Science 6 (2) (1991) 155–168.

[170] T. J. Brukilacchio, A diffuse optical tomography system combined with x-ray mammography for improved breast cancer detection, PhD thesis, TUFTS UNIVERSITY (2003).

[171] V. V. Tuchin, Polarized light interaction with tissues, Journal of biomedical optics 21 (7) (2016) 071114–071114.

[172] J. Selb, T. M. Ogden, J. Dubb, Q. Fang, D. A. Boas, Comparison of a layered slab and an atlas head model for monte carlo fitting of time-domain near-infrared spectroscopy data of the adult head, Journal of biomedical optics 19 (1) (2014) 016010–016010.

[173] S. R. Arridge, W. R. Lionheart, Nonuniqueness in diffusion-based optical tomography, Optics letters 23 (11) (1998) 882–884.

[174] B. C. Van Wijk, C. J. Stam, A. Daffertshofer, Comparing brain networks of different size and connectivity density using graph theory, PloS one 5 (10) (2010) e13701.

Table 1: **fNIRS model assumptions** This table lists assumptions made by popular models used in each data transformation stage. Each assumption a has direct impact in the result of the corresponding stage and should be considered during interpretation.

Stage	Model/Assumption	Consequence	Remedial Action
Image formation and Acquisition	**Radiation transport model (RTE)**:		
	• Ignores light polarization [104, 169]	• This assumption has no significant effect in fNIRS since the polarized state of photons inside the tissue quickly becomes randomized by scattering [170, 171]	
	Diffusion Theory:		
	• Radiant energy does not have a preferential direction of travel	• Inaccurate estimation of light fluence rate like that occurring in regions close to the light source [55]. This is important in cases where a short channel is being considered.	• Use of hybrid methods (Monte Carlo/ Diffusion)
	Anatomical and optical models:		
	• Tissue models based on layered homogeneous slabs	• Biases from estimated spectrum	• Tissue models based in realistic inhomogeneous geometries improves fitting between estimated and measured data [172]
	• Optical properties used in the definition of the forward model (properties measured *in-vivo*, *in-vitro*, etc.) are assumed accurate.	• Inaccuracies lead to biases of the spectra estimated by forward models. • Lack of exact refraction index gets worst the ill-posedness of the inverse problem [173]	• Aggressive regularization techniques may compensate for loss of sensitivity.
Image Reconstruction	**Modified Beer-Lambert Law:**		
	• Light attenuation comes directly from the hemoglobin in the cortex	• Light sensed is contaminated by different sources of noise including the hemoglobin in the scalp blood flow (SBF).	• A common strategy is to regress out the influence of the SBF from a short channel. • Processing techniques reduce contribution from unwanted physiological sources of noise like heart rate or arterial blood pressure [51]

Continued on next page

Table 1 – *Continued from previous page*

Stage	Model/Assumption	Consequence	Remedial Action
	• Attenuation is due only to absorption. Scattering is neglected when determining optical density	• Error in quantification.	• Frequency-domain or time resolved modalities permit separation of absorption and scattering effects.
	• Tissue homogeneity	• Underestimates the amplitude of the changes in oxy- and deoxy- hemoglobin [13]	• Inclusion of PPF (partial pathlength factors) in the MBLL. As the real PPF is difficult to measure *in-vivo*, commonly the DPF (differential pathlength factor) is used instead.
	Perturbation method:		
	• Inverse reconstruction function can be approximated linearly ignoring high order terms in Taylor series.	• The solution is approximated linearly introducing a reconstruction error and affecting sensitivity to parameters.	• Success depends on the effect played by higher-order terms and the initial point[104]. Either higher terms can be used or different models are available.
Analysis	**General Linear Model:**		
	• Errors are independent and identically distributed, following a normal distribution	• The predicted mean may not necessarily be the same as the response distribution's canonical location parameter	• A link function $g(\mu)$ over the structural component $\beta_0 + \beta X$ of the model can be introduced as usually done in the generalized linear model
	• Fitting by least squares	• Strict exogeneity, errors are spherical (homocedastic and non self-correlated)	• Use of mixed effects models, fittings like robust least squares, etc.
	Dynamic Causal Modelling:		
	• Non-systemic brain hemodynamics is purely the effect of brain activity	• Ignoring deviations due to inhibition and underestimating activity	• We are unaware of a specific solution developed for DCM. Carefulness during interpretation must be stressed.
	Graph theoretical models:		
	• Often assume simple graphs as the solutions	• Ignores possible alternative paths for connectivity • Directed graphs alone are insufficient for expressing causality, in principle limiting the analysis of effective connectivity	• Follow advice on how to interpret e.g. [174] • Allow for multiple and/or causal graphs

Continued on next page

Table 1 – *Continued from previous page*

Stage	Model/Assumption	Consequence	Remedial Action
	• Metrics developed for large graphs are still valid for small graphs	• Prunning of non-significant edges may be biased • Graph density may be affected • Network topology e.g. small-world, may appear altered.	• Follow advice on how to interpret e.g. [174]
	Manifold based models:		
	• Compliance with the manifold topology is assumed rather than evidenced.	• With sparse sampling, deviations from the true topology may be substantial.	• Efforts can be made to choose the most likely topology, e.g. using persistent homotopy.
	• The chosen geometrical distance (even geodesic) over the ambient representation characterises the neuroscientific phenomenon of interest	• Altered appreciation of the phenomenon, perhaps even misleading.	• Accompany results with an analysis of the chosen distance. • Ensure a sufficiently dense sampling over the solution manifold to facilitate recovery.